Capillary-Induced Hair Twist

Lauren Kovanko and Sameh Tawfick

Mechanical Science and Engineering, University of Illinois Urbana-Champaign, 1206 W. Green St. Urbana, IL 61801

The Beckman Institute for Advanced Science and Technologies, University of Illinois Urbana-Champaign, 405 N. Matthews Ave, 61801

Abstract

We investigate the self-assembly of hair-like fibers into twisted helices as they are pulled through the liquid interface at a controlled rate. Capillary-induced spontaneous fiber twisting phenomena are observed from the nanoto the millimeter scale. Here, we control the drain rate of the liquid and observe two regimes of self-assembly of long hairs. At low drain rates, the hairs coalesce radially to form a dense aggregate. At higher drain rates, spontaneous hair twisting occurs. We find that the drain rate corresponding to the twisting threshold scales with the characteristic velocity of fiber coalescence set by a balance between liquid viscosity μ and surface energy σ and reads $\sim (\sigma/\mu) \cdot (S/l)^2$ where S and l are the spacing between hairs and their length respectively. At drain rates higher than this threshold, liquid is entrained between the hairs as they emerge from the liquid surface, forming a circular liquid column. Twisting is induced by the fast radial shrinking of this liquid column, combined with the nonlinear resistance to the hairs' radial versus tangential coalescence. Understanding the kinetics is crucial to control this complex self-assembly and to engineer fiber drying processes at various length scales.

Introduction

Long and thin fibers of carbon nanotubes or 3D printed polymer spontaneously self-organize into helical assemblies due to capillary forces as shown in Figure 1. These assemblies are retained due to van der Waals forces after drying. Helical microand nanostructures have potential applications ranging from manipulation of particles and biological cells¹, or in metamaterials such those where the chirality of the helices interacts with circularly polarized light.² Despite their potential significance, the formation of these helices remains difficult to control. This difficulty can be attributed partially to the lack of understanding of the kinetics of their self-assembly. Simple energetic and thermodynamic analyses were used to show that the helical geometry of fiber assemblies balances the bending strain energy and the van der Waals adhesion by maximizing contact. 1,3,4 However, the kinematics of the self-assembly remain obscure due to the challenges of imaging at such small scales and appreciable speeds. In this study, we reveal the critical role of the kinetics of hair-like fibers in their spontaneous self-organization into helices.

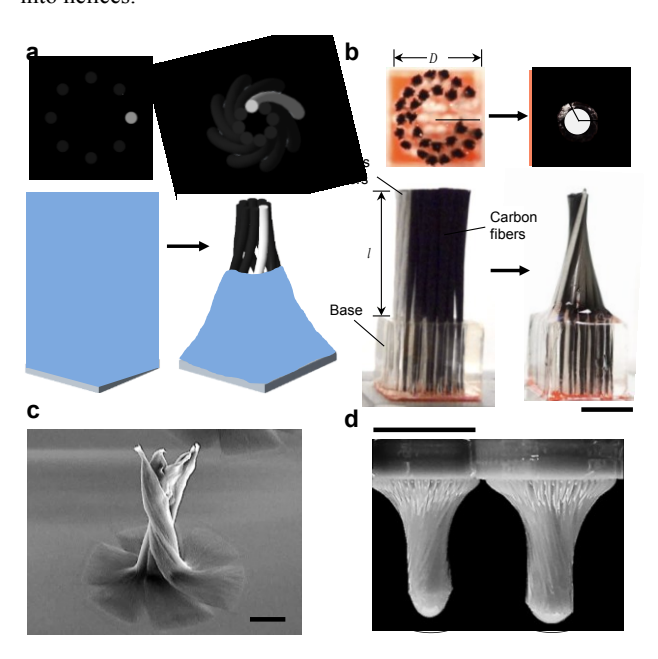


Figure 1. Fibers that twist. a, Fiber schematic top view (top) and side view (bottom) before liquid drainage (left) and twisted after liquid drainage (right). b, Fiber sample top view (top) and side view (bottom) before drainage (left) and after drainage in helical formation (right). White fibers give contrast to and thin lines on top-view images show the twist. Scale bar 1 cm. c, Helical carbon nanotube structure formed by liquid evaporation. Scale bar 10 μm . d, 3D-printed hairs, diameter 250 um, forming helical structures when drawn from resin bath. Scale bar 1 cm.

We have designed new hair assemblies that twist spontaneously when removed from a liquid bath as shown in **Figure 1b**. The hairs are made of carbon fibers, having diameter $d = 5 \mu m$, thus scaling the twisting phenomena by ~100 to 1000 folds compared with nanotubes and nanowires. Thousands of commercially-available carbon fibers are arranged perpendicularly to a base and submerged in an acetone—water solution (see **video S1, S2**), then removed from the liquid using a speed-controlled motorized stage. The fibers pierce the air—liquid interface as they emerge from the bath. The Young's modulus of each fiber is E = 200

GPa. The length of the fibers (l=15–21 mm) is designed to be much larger than the elastocapillary length, $l_{\rm EC}=(Er^3/\sigma)^{1/2}=9.8$ mm, where r is the fiber radius and σ is the surface tension. Above the characteristic elastocapillary length, the fibers will deform due to capillary forces. The spacing among fibers $S\sim200$ μm is much larger than their diameter S>>d, and much smaller than the capillary length ($l_{\rm cap}=1.88$ mm), meaning that the effects of gravity are insignificant compared with those of surface tension. The fibers assemble into bundles of ~1 mm diameter, which is on the same order as $l_{\rm cap}$. As a result, these hairs behave very similarly to nanotubes or nanowires, yet allow high-speed imaging and observation of the kinematics of helices formation.

Interestingly, we find that there exist two regimes of capillaryinduced behavior. The first regime is when the drain rate, set by the speed of the stage, is below a critical or threshold drain rate of $v_d = 3.1$ mm/s. In this regime, the fibers coalesce as their assembly shrinks radially, and no twisting is observed. The second regime occurs when the drain rate is above the threshold drain rate. Within this regime, the fibers self-assemble into helices as shown in Figure 1a,b. This unusual twisting behavior is clearly related to the dynamics of draining liquid, and not static force balance arguments alone. The restoring spring forces of cylindrical fiber assemblies provide the required anisotropy for helical twisting. In particular, the inward radial displacement of fibers is resisted by nonlinear forces due to the successive fiber contact—a behavior reminiscent of foam densification. On the other hand, the tangential twisting of fibers is resisted by a smaller force due to the local bending of fibers. As a result of this anisotropy, the capillary forces can make the fibers twist instead of merely coalescing. At low drain rates, the fibers coalesce to a dense assembly; the liquid film entrained in the bundles is thin and does not allow further fiber mobility or twisting. However, at the threshold drain rate, sufficient liquid is entrained between the fibers to lubricate the assembly, thus providing the kinetic pathway for twisting instead of pure coalescence.

Simple scaling analysis provides useful insight into the threshold drain rate leading to spontaneous twisting. At very low drain rates $(v < v_d)$, the fibers coalesce in the radial direction due to the menisci between the fibers, as seen from the top-down. The rate of this coalescence is limited by the viscous flow of the liquid within the small spacing between the fibers. Below the threshold drain rate, the fibers coalesce radially at a rate controlled by the motion of the stage. We can find this intrinsic coalescent velocity of two plates by considering the balance between the rate of mechanical work done by the capillary forces, F_c , and the rate of energy dissipation by the viscous flow as the plates coalesce and squeeze out the liquid entrained between them.⁶ The rate of work done by the capillary forces scales with the product of the capillary force between two fibers, F_c , and the coalescent velocity, v_c , and scales with $\sim F_c v_c$. The rate of viscous dissipation scales like $\sim \mu(U/S)^2 V$, where μ is the dynamic viscosity of the liquid, U is the flow velocity parallel to the fibers, and V is the volume of entrained liquid. Balancing the rate of work by capillary forces and the viscous dissipation, we obtain $F_c v_c$ $\sim \mu(U/S)^2 V$. Calculating the capillary force as the product of surface tension, σ , and fiber length, l, we can write the balance as $\sigma v_c \sim \mu U^2$. Applying the mass conservation as $v_c/S = U/l$, an expression is obtained for $v_c \sim (\sigma/\mu) (S/l)^2$. Numerically, taking the surface tension of a 50% acetone–water solution $\sigma = 32.33$

mNm⁻¹, dynamic viscosity $\mu = 1.513$ mPa·s, spacing S = 200 μ m, and fiber length l = 21 mm, we estimate the coalescent velocity of the fibers to be on the order of 1 mm/s. Values of liquid constants are obtained from ^{7,8}. This coalescent velocity describes the rate at which two fibers self-assemble radially, and it can be used to estimate the characteristic time scale of the shrinkage of the fiber assembly: $\tau = D/v_c \approx 9$ seconds where D =17.68 mm is the outer diameter of the dry assembly and the initial distance between two fibers before coalescence. The theoretical threshold vertical drain rate at which liquid is entrained before coalescence is $v_d = l/\tau \approx 2.3$ mm/s. Being on the order of a few millimeters per second, this theoretical value agrees well with the threshold drain rate that we observe experimentally of 3.1 mm/s, confirming our hypothesis about the need for a sufficient amount of entrained liquid to lubricate the fibers and form a helical assembly. To further understand this twisting behavior, we use experiments and scaling analysis to capture the role of the drain rate.

Experimental

Samples consist of 30 tows of carbon fibers having length l =15–21 mm organized into rings (**Figure 1b**). The outer diameter of the ring is D = 17.68 mm. Each tow has ~4600 fibers. Four tows at one side of the assembly are made of glass fibers to facilitate the motion tracking. We have confirmed that the glass fibers do not change the results by testing assemblies of carbon fibers only. Each sample is placed on a stationary bracket and submerged in liquid acetone-water solution as shown in Figure 2a. The liquid is then drained from the sample at drain rate v. ranging from 3 to 117 mm/s. During the liquid drainage, the fibers self-assemble in one of two ways. At low drain rates v < v_d , the fibers coalesce radially. At and above the threshold drain rate the fibers twist, forming helices as they coalesce. We measure the twist by tracking the glass fibers observed from the top view as displayed in Figure 2b. We observe that the angle of twist and the twist rate depend on the drain rate, shown in Figures 2c and 2d. The twisted fibers retain their shape, even when the sample has dried due to the coating on the fibers called sizing.⁵ This process is reversible and repeatable; when the fibers are again submerged in the liquid, they return to their original, vertical configuration and the self-assembly process can be repeated (Video S2)

Results and Discussion

We tested samples of various fiber lengths. The shortest sample having fiber length $l=15\,$ mm did not twist for any drain rate. The samples with larger lengths, i.e. $l=17-21\,$ mm, all showed twisting. The angle and twist rate dependence on drain rate for all bundle lengths can be found in the supporting information (**Figure S6**). We observe that the degree of twist and the twist rate are dependent on the fiber length and drain rate. For a constant fiber length, the degree of twist and twist rate increase with increasing drain rate. For a constant drain rate, the degree of twist and twist rate increase with increasing fiber length.

We study the relation between the instantaneous density of the fiber assembly and the tangential velocity. At the instant of peak twist rate of each experiment, we calculate the fiber volume fraction, ϕ , by dividing the total area of fibers by the cross-sectional area of the fiber assembly, shown in **Figure 2e**. When the drain rate is relatively low, the fibers coalesce to a greater extent before twisting, resulting in larger fiber volume fraction

during twisting. For relatively high drain rates, the fibers twist earlier with more liquid entrained between them, hence the volume fraction is lower. As the drain rate is increased further, the volume fraction levels off at this low density value.

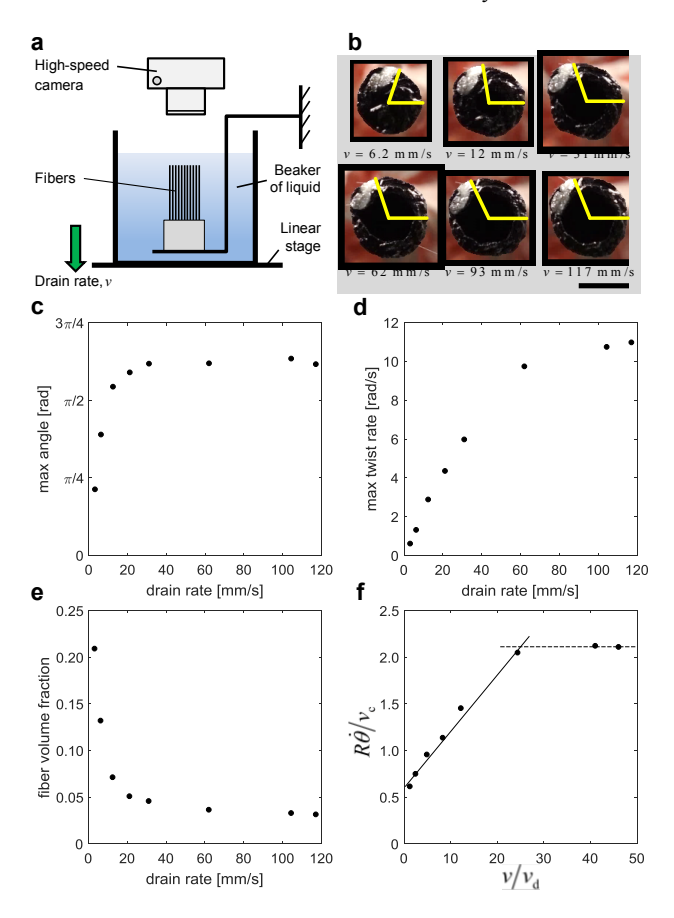


Figure 2. Experimental setup, post-experiment images, angle and angular velocity dependence on drain rate for fiber length 21 mm. a, The fiber sample is fixed in space and submerged in beaker of liquid, which is mounted to a computer-controlled stage. During the experiment, the beaker moves downwards and the liquid is drained from the fibers at speed ν . A high-speed camera captures a top view of the resulting fiber motion. b, Top-view images of the sample after drainage of varying rates. Yellow angles show the maximum angle of twist, measured by position of white glass fibers. Scale bar 5 mm. c, Plot of maximum angle vs. drain rate. d, Plot of maximum twist rate vs. drain rate. e, Plot of fiber volume fraction vs. drain rate. f, Plot of nondimensional maximum twist rate vs. nondimensional drain rate.

Non-dimensionalizing the maximum twist rate vs. drain rate provides insight into the limits of the twisting rate, shown in **Figure 2f**. The x-axis is the ratio of the drain rate to the threshold drain rate, v/v_d . The y-axis is made dimensionless by comparing the maximum tangential velocity of the fiber assembly with its instantaneous coalescent velocity v_c . The tangential velocity is calculated from the experiments as the product of the instantaneous radius of the fiber assembly, R(t), and the maximum twist rate, $\dot{\theta}_{\rm max}$, resulting in $R\dot{\theta}$. The instantaneous radius of the fiber assembly, R(t), changes throughout the experiment due to coalescence; we use the instantaneous radius of the fiber assembly at the moment of peak twist rate, $R(\dot{\theta}_{\rm max})$. This radius depends on the amount of liquid that is entrained between the fibers, which depends on the drain rate of the

experiment; therefore, the radius $R(\dot{\theta}_{\rm max})$ is different for each experiment. The values of v_c are calculated using the instantaneous viscosity and fiber spacing of the liquid-entrained fiber assembly at the time of maximum twist rate. The instantaneous viscosity depends on the fiber volume fraction. This dependence is approximately similar to the viscosity dependence on hard sphere colloids at low volume fraction, $\mu = \mu_0 (1 - \phi/0.63)^{-2}$, where μ is the instantaneous viscosity, μ_0 is the viscosity of the pure liquid, and ϕ is the instantaneous volume fraction. 9 By non-dimensionalizing the twist rate data, we observe a linear trend as v/v_d increases. When v/v_d reaches ~25, the non-dimensionalized data become constant, indicating that the ratio of the fibers' tangential velocity to coalescent velocity stays the same as drain rate increases. Also at this critical ratio of drain rate, the volume fraction becomes constant (Figure 2e, $v \approx$ 62 mm/s), and hence the amount of liquid that the fibers can entrain is maximum and cannot increase further with drain rate, essentially limiting the extent and rate that the fibers are able to twist. This clearly shows that the maximum twisting rate is limited by the intrinsic coalescence velocity v_c . Note that these are scaling arguments, and with the correct pre-factor on the nondimensional twist rate (y-axis), we expect that the limiting twist rate value will be equal to 1.

We analyze the twisting kinematics of fiber length $l=21\,\mathrm{mm}$ at drain rates $v=6.2\,\mathrm{mm/s}$, $v=12\,\mathrm{mm/s}$, and $v=117\,\mathrm{mm/s}$, fiber length $l=19\,\mathrm{mm}$ at drain rate $v=117\,\mathrm{mm/s}$ and fiber length $l=17\,\mathrm{mm}$ at drain rate $v=117\,\mathrm{mm/s}$ (see video S3 to S8). With this selection, we analyze a range of fiber length and drain rate combinations as shown in Figure 3. For each experiment, a reference point at the glass fibers is used to measure the radial and angular position throughout the experiment. This data can be found in Figure S4. From the radius and angle measurements, the radial velocities and angular velocities are calculated. Figure 3 also shows the trajectory of the reference fibers during the experiment and the time dependence of the radial and angular velocities.

The instantaneous radial and tangential velocity are extracted from the videos and plotted versus drain time. These curves are obtained by differentiating the fits to the radius and angle data (see Figure S5). A fit of exponential form fits well to the radius data. We use this form because the viscous damping effect of the liquid causes the radial motion of the fiber to decay exponentially. This damping also affects the twisting motion of the fibers for the case of long fibers, fast drain rate (l = 21 mm, v= 117 mm/s), so the exponential fit is also applied to this angle data, corresponding to Figure 3c. The fit to the angle data of the remaining four cases uses a sigmoid-type logistic function. The logistic fit captures the angle's dependence on the angular velocity, and its derivative fits the bell-shaped increase and decrease in the angular velocity during twisting. It is interesting that a sigmoid-type function—typically used for complex population evolution dynamics—captures the displacement evolution of the fiber assembly.

The kinematics of the observed twisting is dependent on the fiber length and the liquid drain rate. For the various combinations of length and drain rate, the fibers always have initial radial motion before they twist. The amount and rate of the initial radial motion varies between each case. When the fibers are relatively long and the drain rate is relatively low (v = 6.2 mm/s), the radial coalescence and angular motion occur sequentially, and most of the motion is the initial radial coalescence (Figure 3a). When the drain rate increases by approximately a factor of two (v = 12mm/s), the fibers also coalesce before rotating, but the rotation occurs earlier, at smaller radial displacement (Figure 3b). At very fast liquid drainage (v = 117 mm/s), a very brief initial radial assembly is followed by simultaneous coalescence and twist (Figure 3c). As for the various-length study, we observe that the initial radial coalescence increases as the fiber length is decreased (Figure 3d, e).

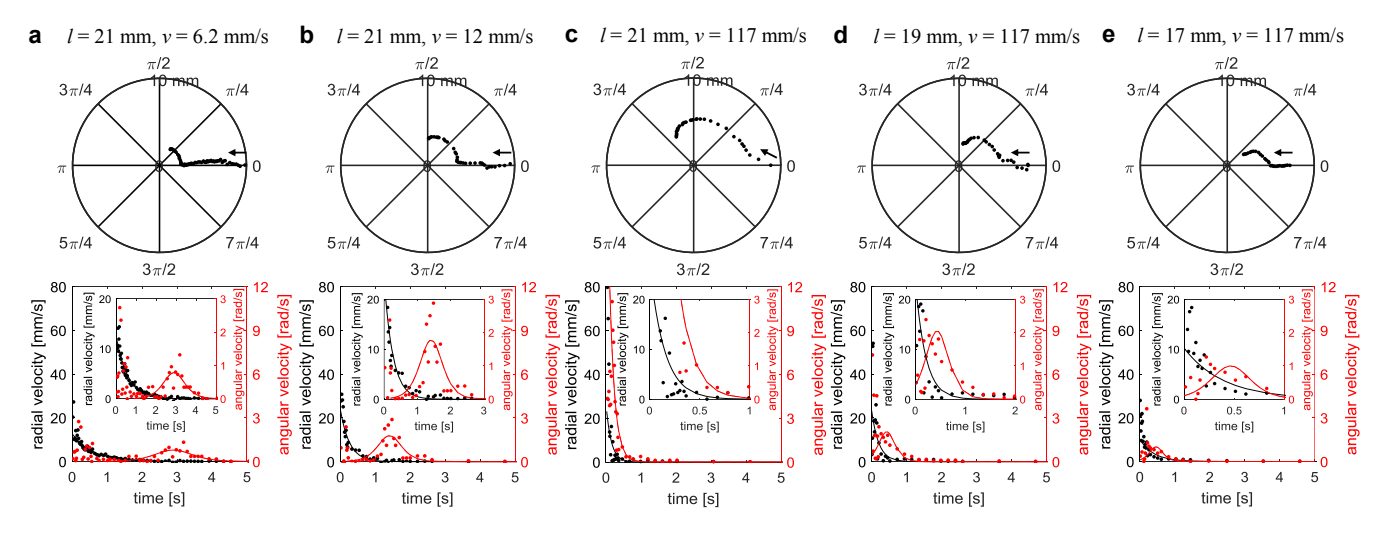


Figure 3. Kinematics of twisting. Trajectory of reference fibers (top), plot of radial velocity on left y-axis, angular velocity on right y-axis, time on x-axis, with inset (bottom) for **a**, fiber length l = 21 mm, drain rate v = 6.2 mm/s. **b**, fiber length l = 21 mm, drain rate v = 12 mm/s. **c**, fiber length l = 19 mm, drain rate v = 117 mm/s. **d**, fiber length l = 19 mm, drain rate v = 117 mm/s.

The radial velocity at the onset of coalescence is on the order of \sim 20–60 mm/s. It increases with the increase in drain rate. The radial velocity of this order is also limited by the viscous drag

within the fiber assembly. At drain rates above the threshold velocity, a column of liquid is formed with the fibers acting as a scaffold for the liquid as shown in videos S3 to S7. In this case,

the radial coalescence is driven mostly by the menisci between two fibers along their length. The flow of the entrained liquid perpendicular to the fibers can be modeled as perpendicular flow through a square array of cylinders. To find the perpendicular velocity, U_{\perp} , we balance the drag force per unit length of the fiber with the capillary force per unit length. The drag force per unit length scales like $(\mu U_{\perp}/\epsilon)k$, where μ is the viscosity of the acetone-water solution, ε is the void fraction, and k is the Kozeny constant.¹⁰ Knowing the dimensions of the ring sample and its number of fibers, the void faction $\varepsilon = 0.988$. The Kozeny constant for our case of extremely low fiber volume fraction is k= $-2/[(1-\epsilon)\ln(1-\epsilon)]$, given in reference ¹⁰ as a simplified equation for Eqn. (24) for the case of low volume fraction. Substituting this expression for k into the expression for the drag force and balancing with the capillary force per unit length, we arrive at the result that $U_{\perp} = -\sigma[(1-\varepsilon)\ln(1-\varepsilon)]/(8\pi\mu)$. Using the known values of σ and μ for 50% acetone—water solution, we can theoretically estimate that $U_{\perp} \approx 45$ mm/s, which is close to the peak radial velocity observed. This confirms that at high drain rate, the rate of coalescence is limited by the drag of flow through the fiber array.

By studying the kinematics of fibers during liquid drainage, we identify the forces that drive the self-assembly. Twisting is an instability that stems from asymmetry in fiber arrangement, capillary force direction, and fluid flow within the fibers. Any small imperfection causes the capillary force to have an offset angle from the pure radial forces expected for the ideal fiber bundles. The tangential component causes a "twisting torque," reminiscent of the effect of offset forces on the lateral buckling of elastic columns. The twisting torque and the intrinsic smaller resistance to rotation than radial coalescence lead to the twisting instability. For this self-organization to take place, the fibers must be sufficiently lubricated as demonstrated by the ratecontrolled experiments. If the liquid is drained too slowly, the fibers establish contact before they have sufficient time to twist. The contact friction and surface adhesion eliminate the twisting instability. On the other hand, when the drain rate is above the threshold value, liquid remains entrained as the capillary force assembles the fibers (Figure 4a). As the assembly shrinks, the fibers become crowded and feel more resistance to motion in the radial direction than the tangential direction, leading to twist (Figure 4b). These insights are validated by the experimental observation of the twist rate dependence on the drain rate.

We formulate a nonlinear force law to capture the complex resistance to the fibers' coalescence. A free-body diagram of the fiber is shown in **Figure 4c**. We model the motion of a single fiber of mass m subject to radial capillary force F_c with an offset angle α . We write a full equation of motion taking into consideration the fiber mass, nonlinear stiffness, and draginduced damping. Equation (1) is the equation of radial fiber motion, and equation (2) is the equation of tangential fiber motion. We still write an inertia term in the equation of motion as it has negligible effect on the results due to the fiber's size. The initial conditions that the fiber is given are the experimentally-determined initial positions and velocities.

$$m\ddot{r} = \left(F_{\rm kn} + F_{\rm kf,r}\right) \left[\frac{r_0 - r_{\rm D}}{r - r_{\rm D}}\right]^n + F_{\rm centripetal} + F_{\rm D,r} + F_{\rm capillary,r} \tag{1}$$

$$mr\ddot{\theta} = F_{kf,\theta} + F_{coriolis} + F_{D,\theta} + F_{capillary,\theta}$$
 (2)

The forces that resist the motion of the fiber are the nonlinear force in the radial direction, $F_{\rm kn}$, resulting from the successive contacts of the fibers as they assemble, and the linear force, $F_{\rm kf}$ resulting from the cantilever stiffness of the single fiber (**Figure S7**). The forces $F_{\rm Dr}$ and $F_{\rm D\theta}$, in the radial and tangential directions, respectively, are viscous drag forces that also resist the fiber motion. The force $F_{\rm kn}$ is represented by a nonlinear spring connecting the fiber to the origin, having equilibrium at t=0 when $r=r_0$. The nonlinear radial stiffness is proportional to the square of the radial displacement (**Figure S8**). The force $F_{\rm kf}$ stems from a linear spring connecting the fiber's initial position to its current position with stiffness equal to its cantilever bending stiffness. These two springs store the fiber's elastic energy as it deforms.

To further account for the effect of fiber densification and compaction as the fibers crowd, we multiply a dimensionless fiber densification factor by the two spring forces in the radial direction. The form of the densification factor is that of the force-displacement relation of the compression of cellular foams. 11 The densification factor diverges when the fibers are fully dense to capture the transition from low-density foam to a dense solid (see **Figure S9**). In the densification factor, r_0 , r(t), and $r_{\rm D}$, are the initial radial position, instantaneous radial position, and the radial position of complete densification of the fiber, respectively. The values of r_0 and r_D are determined experimentally; $r_{\rm D}$ is the smallest observed radius for a given fiber length. The complex rheology of the lubricated fiber assembly is captured by introducing an exponent, n, on the fiber densification term to modulate the densification rate. The values of term F_{kf} and F_{kn} are estimated from the modulus, dimensions, and spacing between fibers as detailed in the SI (Figure S7); these values are used in all the numerical simulations. The capillary force is calculated by $F_c = 2\pi\sigma(d/2)^2 \cos^2\theta/(S^2 - 4(d/2)^2)^{1/2}$, where d is the diameter of a fiber cluster, θ is the contact angle between the liquid and the fiber 12 and S is the separation between clusters, leading to $F_{\rm c} \sim 10^{-7}$ N. The viscous drag forces $F_{\rm Dr}$ and $F_{\mathrm{D}\theta}$ are $\mu D \dot{r}$ and $\mu D r \dot{\theta}$ respectively, where D is the diameter of the fiber ring assembly, leading to $\mu D \sim 10^{-5}$ Ns/m.

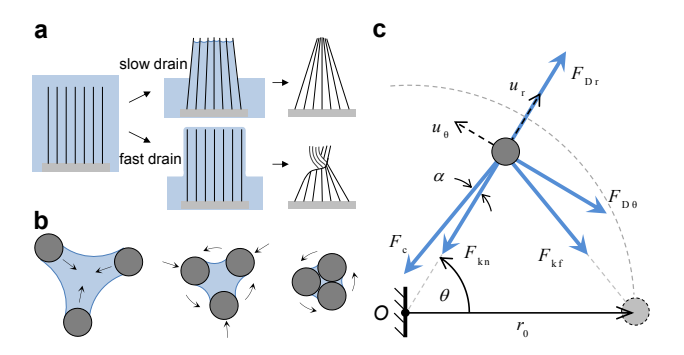


Figure 4. Modeling twisting hairs. a, Schematic of showing effect of low drain rate (below threshold) vs. fast drain rate (above threshold). b, Schematic of fibers coalescing and twisting due to radial and tangential forces. c, Free-body diagram of a single fiber showing forces: capillary force, F_{c} ; nonlinear spring force, F_{kn} ; linear spring force, F_{kn} ; radial drag force, F_{Dr} ; tangential drag force, $F_{D\theta}$.

We numerically solve the differential equations using the conditions of **Figure 3a**, **c**, corresponding to long fiber length and low and high drain rates respectively. As shown in **Figure 5a**, the model captures very well the two-regime self-assembly

behavior consisting of pure radial coalescence followed by pure rotation observed experimentally in the slow drain case. For the case of very fast drain rate (Figure 5b), the numerical solution also predicts the two-regime kinematics, demonstrating the fidelity of the model. More details of the model parameters are listed in the SI (**Table S1**). In the model, the value of F_c is constant, which is an approximation. In reality, the value of F_c depends on the exact shape of the meniscus and spacing between fibers and is constantly changing. The constant value used in the model causes the tangential velocity in the numerical model to keep a finite value at the end of the simulation because the model does not take into consideration the drying of fibers after drainage. However, the model still describes the kinematics of motion with good fidelity and provides valuable insights. The numerical solutions also confirm that, as expected, without introducing an offset angle α only radial coalescence is observed. On the other hand, twisting is obtained in the numerical model for any angle $\alpha > 0$. We also observe that the offset angle affects the timescale of the twisting along with the fiber stiffness and drag forces.

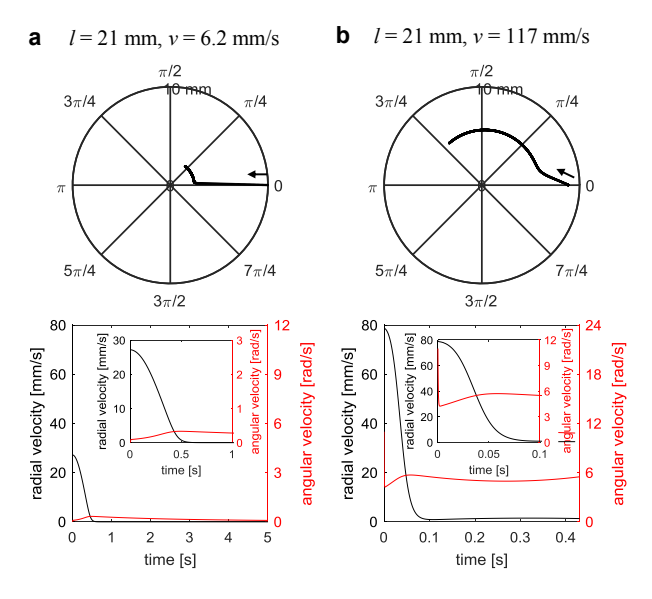


Figure 5. Model-predicted kinematics. Fiber trajectory (top) and plot of radial velocity vs. time and angular velocity vs. time (bottom) for **a**, fiber length l = 21 mm and drain rate v = 6.2 mm/s. **b**, fiber length l = 21 mm and drain rate v = 117 mm/s.

Conclusion

Using simple draining experiments, we have observed and studied the capillary-induced twisting of slender fiber bundles. In the experiments, we control the drain rate and observe the kinematics of fiber twisting. Most notable, we observe that twisting occurs at high drain rates. We also observe that the fibers initially coalesce radially and then twist by rotating in the tangential direction.

We use scaling arguments to demonstrate that the threshold velocity can be related to the characteristic coalescence rate of two fibers in a viscous fluid. We also show that the non-dimensional twisting rate saturates at the value of the coalescence rate. We constructed a simple first-order numerical model that captures the twisting kinematics reasonably well. The

model considers only a single fiber, and replaces the effect of the other fibers in the bundle by appropriate stiffness laws in the radial and tangential directions. An interesting study would be the stability analysis of the radially-coalescing fibers and the emergence of twisting behavior. Nonetheless, this study provides clear evidence on the dynamic nature of twisting and could lead to more controlled nano-pillar and nano-tube twisting self-assembly by controlling the drying rate.

Supporting Information

Experimental details and supplementary figures Video 1/8 showing experimental setup Video 2/8 showing repeated cycles of twisting/untwisting Video 3/8 showing experiment of l=21 mm, v=6.2 mm/s Video 4/8 showing experiment of l=21 mm. v=12 mm/s Video 5/8 showing experiment of l=21 mm. v=117 mm/s Video 6/8 showing experiment of l=19 mm. v=117 mm/s Video 7/8 showing experiment of l=17 mm. v=117 mm/s Video 8/8 showing experiment of l=15 mm. v=117 mm/s

Acknowledgment

The authors acknowledge partial support from NSF CMMI #1825758 and the AFOSR Young Investigator Program FA9550-19-1-0010. L.K. acknowledges partial support from the department of Mechanical Science and Engineering at the University of Illinois.

References

- (1) Pokroy, B.; Kang, S. H.; Mahadevan, L.; Aizenberg, J. Self-Organization of a Mesoscale Bristle into Ordered, Hierarchical Helical Assemblies. *Science* (80-.). 2009, 323 (5911), 237–240. https://doi.org/10.1126/science.1166087.
- (2) Rill, M. S.; Linden, S.; Gansel, J. K.; Thiel, M.; Decker, M.; Bade, K.; von Freymann, G.; Saile, V.; Wegener, M. Gold Helix Photonic Metamaterial as Broadband Circular Polarizer. *Science* (80-.). 2009, 325 (5947), 1513–1515. https://doi.org/10.1126/science.1177031.
- (3) Hu, Y.; Lao, Z.; Cumming, B. P.; Wu, D.; Li, J.; Liang, H.; Chu, J.; Huang, W. Laser Printing Hierarchical Structures with the Aid of Controlled Capillary-Driven Self-Assembly. 2015, 112 (22), 1–6. https://doi.org/10.1073/pnas.1503861112.
- (4) Lao, Z.; Hu, Y.; Zhang, C.; Yang, L.; Li, J.; Chu, J.; Wu, D. Capillary Force Driven Self-Assembly of Anisotropic Hierarchical Structures Prepared by Femtosecond Laser 3D Printing and Their Applications in Crystallizing Microparticles. 2015, No. 12, 12060– 12069. https://doi.org/10.1021/acsnano.5b04914.
- (5) Shin, D.; Tawfick, S. Polymorphic Elastocapillarity: Kinetically Reconfigurable Self-Assembly of Hair Bundles by Varying the Drain Rate. *Langmuir* 2018, 34 (21), 6231–6236. https://doi.org/10.1021/acs.langmuir.8b00593.
- (6) de Gennes, P.-G.; Brochard-Wyart, F.; Quéré, D. Capillarity and Wetting Phenomena; 2004.

- https://doi.org/10.1007/978-0-387-21656-0.
- (7) Howard, K. S.; McAllister, R. A. Surface Tension of Acetone-Water Solutions Up to Their Normal Boiling Points. AIChE J. 1958, 3 (3), 325–329. https://doi.org/10.1002/aic.690040326.
- (8) Howard, K. S.; McAllister, R. A. The Viscosity of Acetone-Water Solutions Up To Their Normal Boiling Points. *AIChE J.* **1958**, *4* (3), 362–366.
- (9) Sjögren, L. Chapter 9: Colloidal Suspensions. Stoch. Process. (Lecture Notes, Gothenburg) 1940, 101–130.
- (10) Happel, J. Viscous Flow Relative to Arrays of Cylinders. *AIChE J.* **1959**, *5* (2), 174–177.
- (11) Ben-Dor, G.; Cederbaum, G.; Mazor, G.; Igra, O. Well Tailored Compressive Stress-Strain Relations for Elastomeric Foams in Uni-Axial Stress Compression. *J. Mater. Sci.* **1996**, *31* (4), 1107–1113.
- (12) Chandra, D. Capillary Force in High Aspect-Ratio Micropillar Arrays. **2009**.

